Chem. Res. Chinese Universities, 2020, 36(6), 1083—1090 doi: 10.1007/s40242-020-0301-1

Article

Enhanced Visible-light Photocatalytic Activity of g-C_3N_4/Nitrogen-doped Graphene Quantum Dots/TiO_2 Ternary Heterojunctions for Ciprofloxacin Degradation with Narrow Band Gap and High Charge Carrier Mobility

CHEN Ting[1], ZHONG Lei[1], YANG Zhen[1], MOU Zhigang[1*], LIU Lei[1], WANG Yan[1], SUN Jianhua[1*] and LEI Weiwei[2*]

1. School of Chemistry and Environmental Engineering, Institute of Advanced Functional Materials for Energy, Jiangsu University of Technology, Changzhou 213001, P. R. China;

2. Institute for Frontier Materials, Deakin University, Waurn Ponds, Victoria 3216, Australia

Abstract Limited visible-light absorption and high recombination rate of photogenerated charges are two main drawbacks in g-C_3N_4-based photocatalysts. To solve these problems, g-C_3N_4/nitrogen-doped graphene quantum dots (NGQDs)/TiO_2 ternary heterojunctions were facilely prepared *via* a one-step calcining method. The morphology, structure, optical and electrochemical properties of g-C_3N_4/NGQDs/TiO_2 were characterized and explored. The optimal g-C_3N_4/NGQDs/TiO_2 composite exhibits enhanced photocatalytic degradation performance of ciprofloxacin (CIP) compared with the as-prepared g-C_3N_4, TiO_2(P25) and g-C_3N_4/TiO_2 heterojunction under visible light irradiation. The apparent rate constant of the composite is around 6.43, 4.03 and 2.30 times higher than those of g-C_3N_4, TiO_2 and g-C_3N_4/TiO_2, respectively. The enhanced photocatalytic efficiency should be mainly attributed to the improvement of light absorption and charge separation and transfer efficiency, originating from the narrow band gap and high charge carrier mobility. The active species trapping experiments results showed that the h^+ and $^{\bullet}O_2^-$ were the main active species in the degradation process. A possible photocatalytic reaction mechanism of the g-C_3N_4/NGQDs/TiO_2 composite for the enhanced degradation of CIP under visible light irradiation was also proposed.

Keywords g-C_3N_4/NGQDs/TiO_2; Heterojunction; Photocatalysis; Antibiotic ciprofloxacin

1 Introduction

Antibiotics as a type of antimicrobial have been widely used to treat bacterial infection. However, with the deliberate discharge of antibiotics in the environment, they have been detected in various ecosystems from terrestrial to aquatic environments, which pose serious risks to human and veterinary health[1]. Moreover, some antibiotics, such as ciprofloxacin (CIP), are considerably persistent and hard to be completely degraded or removed through conventional wastewater treatment technologies, such as adsorption, hydrolysis and chemical oxidation, resulting in their remaining for longer in the environment[2]. It is necessary to develop an effective treatment technology for the degradation of antibiotics. Photocatalysis as one of the most promising methods for degrading the antibiotics has received considerable attention because it is an efficient, environmentally clean and economic technology only using sunlight and appropriate photocatalyst, even though it still remains a huge challenge in the practical application[3].

More recently, graphite-like environmentally friendly carbon nitride(g-C_3N_4) is becoming the focus of research in the field of visible-light photocatalysis owing to its tunable electronic structure, relatively narrow band gap(*ca.* 2.7 eV) and high stability, etc.[4,5]. However, photocatalytic activity for environmental remediation by single g-C_3N_4 is restricted by the limited visible-light absorption(absorption maximum at 460 nm) and high recombination rate of photogenerated charges[6]. TiO_2 is one of the most widely used photocatalysts due to its low cost, nontoxicity, high photoreactivity and chemical stability[7]. P25, as a well-known commercial catalyst containing anatase and rutile phases of TiO_2, is widely used in the degradation of many organic pollutants and antibiotics[8,9]. However, it possesses drawbacks of wide band gap(3.2 eV for anatase, 3.0 eV for rutile) and fast recombination of the photo-induced electron hole pairs, which limit the photocatalytic capability.

*Corresponding authors. Email: jsmzg@jsut.edu.cn; sunjh@jsut.edu.cn; weiwei.lei@deakin.edu.au

Received September 27, 2020; accepted November 17, 2020.

Supported by the National Natural Science Foundation of China(No.21373103), the Natural Science Foundation of Jiangsu Province, China(No.BK20170316) and the PhD Research Startup Foundation of Jiangsu University of Technology, China (No.KYY18038).

Construction of heterojunctions with two semiconductors with suitable band structure is a promising approach for achieving improved photoactivity. According to previous reports[9—12], the g-C_3N_4/TiO_2 heterojunctions usually exhibit superior photoactivity than single photocatalyst due to the high energy difference between the conduction and valence bands of the g-C_3N_4 and TiO_2, resulting in the irreversible spatial charge separation across the heterojunctions and suppression of the recombination of photogenerated holes and electrons[13]. However, these g-C_3N_4/ TiO_2 heterojunctions displayed an obvious blue shift in the absorption edge compared to pure g-C_3N_4 due to wide band gap of TiO_2 in the hybrids. Even though the heterojunctions were in favor of improving separation efficiency of photogenerated carriers, the efficiency of pollutant degradation by g-C_3N_4/TiO_2 heterojunctions was still not satisfactory because of the poor visible-light absorption. Therefore, it is highly desirable to construct the g-C_3N_4 and TiO_2 heterojunctions to combine the extended visible-light absorption capability and highly promote the photogenerated charge separation efficiency.

Graphene quantum dots(GQDs) with a lateral size smaller than 100 nm including single- or few-layered graphene, have drawn much attention owing to their high biocompatibility, good conductivity and excellent photochemistry properties[14,15]. The construction of composite photocatalysts by coupling g-C_3N_4 with GQDs is an effective approach to improve the visible light photocatalytic degradation of contaminants[16,17]. Nitrogen-doping can modulate the electronic properties of GQDs and introduce the “activation region” on the GQDs surface[18,19]. More importantly, based on our previous work[20], the amino groups of nitrogen-doped graphene quantum dots (NGQDs) can provide the ideal sites for tethering to urea-derived g-C_3N_4 by a deamination reaction during thermal condensation, resulting in the formation of new energy bands and an extended visible-light response range in g-C_3N_4/NGQDs heterojunction[20].

Herein, we focused on the integration of g-C_3N_4 with NGQDs and TiO_2(P25) and constructed ternary g-C_3N_4/ NGQDs/TiO_2 heterojunctions by the facile one-step heat treatment of the mixture of P25, NGQDs and urea precursor. The heterojunction photocatalysts can retain the desired characteristics of high utilization of visible light and low recombination rate of photogenerated electron-hole pairs. Compared with the binary g-C_3N_4/TiO_2 heterojunction, the introduction of NGQDs could not only further promote photogenerated charge separation *via* electron injection from g-C_3N_4 to NGQDs, then to TiO_2, but also lead to a red-shift of band gap compared to pure g-C_3N_4. The photocatalytic performance was evaluated by the degradation of CIP under visible light irradiation($\lambda \geqslant 420$ nm). The results exhibited that the as-prepared g-C_3N_4/NGQDs/TiO_2 sample could significantly enhance the photocatalytic activity in comparison with pure g-C_3N_4, commercial P25 and g-C_3N_4/ TiO_2 heterojunction under visible light irradiation. The synergetic effect on the improved photocatalytic performance and a possible mechanism for the degradation of CIP were discussed.

2 Experimental

2.1 Sample Preparation

2.1.1 Synthesis of NGQDs

The NGQDs were prepared referring to the method previously reported with minor modifications[21]. Typically, 0.42 g (2 mmol) of citric acid and 0.36 g(6 mmol) of urea were dissolved into 20 mL of water under magnetically stirring. The resulting clear solution was transferred into a Teflon-lined stainless steel autoclave with a capacity of 50 mL and heated at 160 °C for 4 h. The resulting product was collected by centrifugation at 8000 r/min for 20 min after adding ethanol to the solution, and then dried under vacuum at 50 °C.

2.1.2 Synthesis g-C_3N_4/NGQDs/TiO_2 Composites

The g-C_3N_4/NGQDs/TiO_2 composites were prepared by a one-step calcining method. In a typical preparation procedure, 10 g of urea and 0.5 g of P25 were dispersed into NGQDs aqueous solution(6 mg of NGQDs) under magnetically stirring for 2 h, and then were concentrated by vaporizing the water at 100 °C. After that, the dried mixture was put into a crucible with a cover and then calcined in a muffle furnace at 550 °C for 3 h with a heating rate of 15 °C/min. The resultant sample was cooled to room temperature, grounded into a fine powder, in which the mass ratios of P25 to urea and NGQDs to urea were 5:100 and 6:10000 in the precursors, respectively. The obtained sample was labeled as g-C_3N_4/NGQDs/TiO_2 for simplicity. For comparison, the other ternary composite samples with different mass ratios of P25:urea and NGQDs:urea were also prepared by changing the relative amount of P25 and NGQDs in the precursors. The specific proportions are listed in Table 1. In addition, the sample with mass ratios of P25:urea being 5:100 and NGQDs:urea being 0 was denoted as g-C_3N_4/TiO_2 for simplicity. Pure g-C_3N_4 was also prepared by a similar method as g-C_3N_4/NGQDs/TiO_2 composite without adding NGQDs and P25.

Table 1 Influence of different mass ratios of P25:urea and NGQDs:urea in the preparation of g-C_3N_4/ NGQDs/TiO_2 composite on the photocatalytic activities for CIP degradation

Entry	*m*(P25):*m*(urea)	*m*(NGQDs):*m*(urea)	Activity*(%)
1	0	6:10000	39.7
2	1:100	6:10000	51.9
3	3:100	6:10000	68.2
4	5:100	6:10000	88.0
5	10:100	6:10000	48.3
6	5:100	0	54.2
7	5:100	1:10000	59.0
8	5:100	2:10000	62.2
9	5:100	4:10000	74.3
10	5:100	8:10000	64.2

* Degradation rate after visible light irradiation for 100 min

2.2 Characterization

The morphology of g-C_3N_4/NGQDs/TiO_2 sample was observed on a field-emission scanning electron microscope (FESEM, Sigma, Zeiss) and a transmission electron microscope

(TEM, JEM-2100, Japan). X-Ray diffraction(XRD) patterns were recorded on a Philips diffractometer by using Ni-filtered Cu *Kα* radiation. Thermogravimetric analysis(TGA) was performed in a DSC 404F3 differential scanning calorimeter (NETZSCH, Germany) at a heating rate of 10 °C/min in the air. UV-Vis diffuse reflectance spectra were measured on a Hitachi UV-3010 spectrophotometer using $BaSO_4$ as a reflectance sample. X-Ray photoelectron spectroscopy(XPS) measurements were carried out by an AXIS Ultra DLD system(Kratos Analytical Inc.) with an Al *Kα* X-ray radiation source. The photoluminescence(PL) spectra were obtained on an Edinburgh FLS920 fluorospectrophotometer with an excitation wavelength of 370 nm. The electrochemical impedance spectroscopy (EIS) was tested on a CHI 660B electrochemical workstation by using a standard three-electrode configuration consisting of the prepared samples as the working electrodes, a saturated Ag/AgCl electrode as the reference electrode and a platinum wire as the counter electrode. The electrolyte was a 0.5 mol/L Na_2SO_4 aqueous solution. The EIS was measured under the perturbation signal of 5 mV over the frequency range from 1 MHz to 100 MHz. The working electrodes were prepared as follows: 10 mg of sample powder was thoroughly mixed with 2.0 mL of ethanol solution of Nafion(0.02%) to form a slurry, and the obtained slurry was applied evenly onto 1 cm^2 of a conducting indium tin oxide glass substrate to form a film with a thickness of around 10 μm. After air-drying, the working electrodes were further dried at 80 °C for 3 h to improve the adhesion.

2.3 Photocatalytic Activity Test

Photocatalytic degradation was performed in a top-irradiation quartz reaction vessel connected to a circulating water system to maintain at room temperature. The photocatalytic activities were investigated by the degradation of CIP aqueous solution under visible light irradiation. The visible light source was provided by a 300 W Xe lamp equipped with a 420 nm cutoff filter(irradiation intensity: *ca.* 98 mW/cm^2). In a typical experiment, 50 mg of g-C_3N_4/NGQDs/TiO_2 sample was added to a 100 mL of CIP(10 mg/L) aqueous solution and stirred in the dark for 30 min to achieve adsorption-desorption equilibrium between the photocatalyst and CIP. During irradiation, 3 mL of suspension was taken out at certain time intervals and centrifuged at 10000 r/min for 3 min to remove the catalyst particulates. The residual concentrations of CIP were analyzed by recording variations of the characteristic absorption band of 272 nm using a UV-Vis spectrophotometer(Agilent, Cary-100).

For further identifying the generated active species during the reaction process of g-C_3N_4/NGQDs/TiO_2, isopropyl alcohol (IPA), *p*-benzoquinone(BQ) and disodium ethylenediaminetetraacetate(EDTA-2Na) were used as hydroxyl radical($^{\bullet}OH$), superoxide radical($^{\bullet}O_2^-$) and holes(h^+) scavenger, respectively. The scavenger with a concentration of 10 mmol/L was added respectively to the CIP solution to probe the active species through the variation of degradation rate.

3 Results and Discussion

3.1 Morphology and Structure

The morphological structure of the composite was investigated by taking FESEM, TEM and HRTEM images of g-C_3N_4/NGQDs/TiO_2 sample. As can be seen from FESEM in Fig.1(A), g-C_3N_4 presents an obvious two-dimensional lamellar structure with the agglomeration of P25 on the surface of g-C_3N_4. TEM image[Fig.1(B)] further shows the P25 nanoparticles with sizes ranging from 20 nm to 30 nm are uniformly dispersed on the surface of g-C_3N_4. Fig.1(C) gives the corresponding HRTEM image. The distinct lattice fringes with the spacings of 0.35 and 0.24 nm are related to the crystallographic planes of the anatase TiO_2(101) and NGQDs(1120), respectively. As displayed, a triple junction exists among g-C_3N_4, NGQDs and P25 in the as-prepared g-C_3N_4/NGQDs/TiO_2 composite. This well contacted triple heterojunction is beneficial for charge transfer to improve the photocatalytic degradation of CIP.

Fig.2 shows the XRD patterns of pure g-C_3N_4, TiO_2(P25), g-C_3N_4/TiO_2 and g-C_3N_4/NGQDs/TiO_2 samples. For pure g-C_3N_4, two main diffraction peaks at approximately 2θ=27.2° and 13.1° can be observed, corresponding to the (002) and (100) plane diffractions of g-C_3N_4, respectively[22]. As can be seen, g-C_3N_4/TiO_2 and g-C_3N_4/NGQDs/TiO_2 samples exhibit similar XRD patterns with pure P25. The peaks of 2θ=25.3°, 37.8°, 48.0°, 54.0°, 55.1°, 62.6° and 75.1° correspond to the (101), (004), (200), (105), (211), (204) and (215) crystal planes of anatase TiO_2 in P25, respectively. In addition, the peaks of 2θ=27.3°, 36.1° and 41.2° are also observed, which correspond to the (110), (101) and (111) crystal planes of rutile TiO_2 in P25, respectively[23]. No characteristic diffraction peaks of g-C_3N_4 and NGQDs are observed due to the relatively low crystallinity of g-C_3N_4 and low amount of NGQDs(see TGA result below). Similar results have also been reported by other authors[24,25]. It is clear to find that the addition of g-C_3N_4 and NGQDs almost have no effect on the crystallinity of TiO_2(P25).

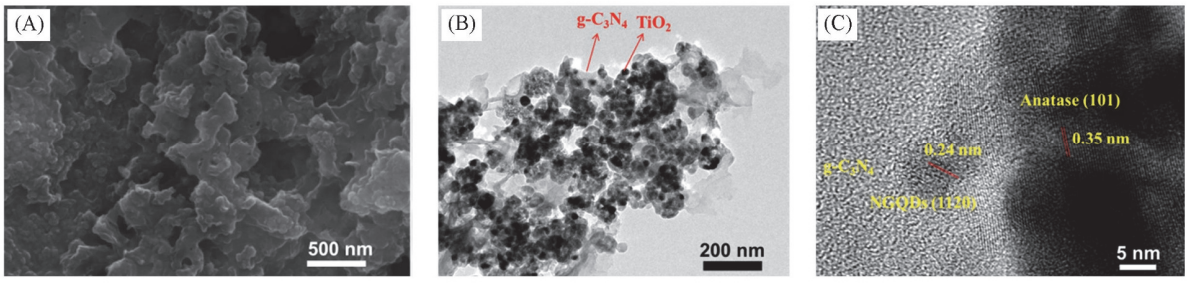

Fig.1 FESEM(A), TEM(B) and HRTEM(C) images of g-C_3N_4/NGQDs/TiO_2 sample

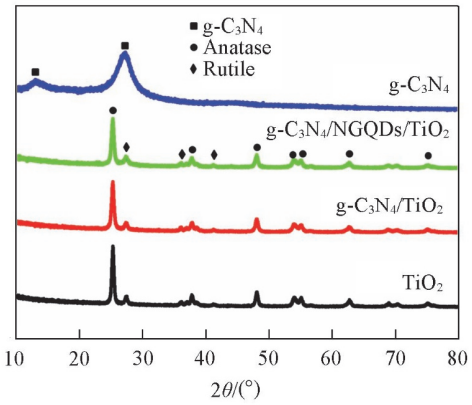

Fig.2 XRD patterns of pure g-C_3N_4, TiO_2(P25), g-C_3N_4/TiO_2 and g-C_3N_4/NGQDs/TiO_2 samples

TGA measurements in the air were carried out to ascertain the composition and thermostability of g-C_3N_4/NGQDs/TiO_2 composite. As shown in Fig.3, g-C_3N_4 was thermally stable below *ca*. 500 °C, while it could be completely decomposed when the temperature was higher than 700 °C in the air. On the contrary, TiO_2(P25) exhibits very low mass loss in the TGA curve due to its high thermostability. For the g-C_3N_4/NGQDs/TiO_2 sample, when the temperature was up to 400 °C, it began to lose mass, and then reached a steady state when the temperature was higher than 500 °C, which indicated that the combustion of g-C_3N_4 and NGQDs took place from 400 °C to 500 °C. It could be seen that the thermal stability of the g-C_3N_4/NGQDs/TiO_2 sample was decreased because that NGQDs would catalyze the decomposition of g-C_3N_4 at a relatively low temperature[26]. The mass loss below 200 °C is mainly due to the evaporation of water, so the content of NGQDs+g-C_3N_4 in the sample was calculated from the mass remainder in the temperature range of 200—1000 °C. The content of NGQDs+g-C_3N_4 in g-C_3N_4/NGQDs/TiO_2 was about 32%. Since TiO_2 (P25) was thermally stable, the mass fractions of g-C_3N_4 and NGQDs were calculated to be about 31.2% and 0.8%, respectively, based on the assumption of the fixed mass of NGQDs during the preparation of the sample.

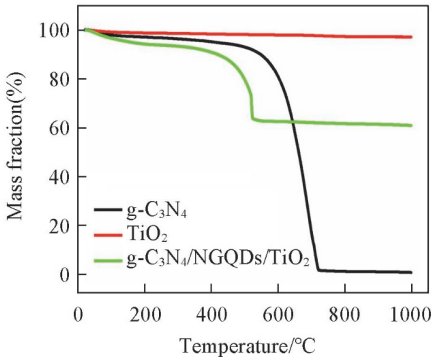

Fig.3 TGA curves of pure g-C_3N_4, TiO_2(P25) and g-C_3N_4/NGQDs/TiO_2 samples

XPS was utilized to investigate the chemical compositions and status of the as-prepared samples, as shown in Fig.4. Fig.4(A) lists the XPS survey spectra of the g-C_3N_4/NGQDs/TiO_2 and pure g-C_3N_4, in which four elements C, N, Ti and O are observed in the g-C_3N_4/NGQDs/TiO_2 sample, and only C, N and a small amount of O originating from the adsorbed H_2O on the surface exist in pure g-C_3N_4. Fig.4(B) is the high-resolution spectra of the C_{1s}. As revealed by Fig.4(B), three obvious peaks at 284.6, 288.0 and 293.7 eV are observed for g-C_3N_4, which are related to aromatic carbon atoms, sp^2-bonded carbon(N═C—N_2) in the triazine rings and the carbon in aromatic rings connected with the terminal uncondensed NH_2 species[27], respectively. For g-C_3N_4/NGQDs/TiO_2, the intensity of the peak at 284.6 eV increased with the appearance of a new peak at 285.9 eV corresponding to the C—O bond compared with pure g-C_3N_4. These results originate from the aromatic carbon atoms and oxygen-containing functional groups on NGQDs, indicating the incorporation of NGQDs into the heterojunction. Fig.4(C) exhibits the N_{1s} in pure g-C_3N_4 and g-C_3N_4/NGQDs/TiO_2 samples. In the deconvoluted N_{1s} spectrum of pure g-C_3N_4, four peaks at about 398.4, 398.9, 400.5 and 404.5 eV can be assigned to sp^2 hybridized N(C═N—C), tertiary N groups(N—C_3), N—H bonds, and the π excitations, respectively[20,28]. For g-C_3N_4/NGQDs/TiO_2 sample, the four peaks all shift to higher values compared with pure g-C_3N_4, indicating the strong interaction between g-C_3N_4 and NGQDs(or TiO_2). Similar shifts were also observed in g-C_3N_4/NGQDs composite in our previous report[20]. The introduction of oxygen-containing materials(NGQDs and TiO_2) in the framework of g-C_3N_4 may result in the formation of electron-withdrawing groups tethering to the aromatic skeleton rings. The XPS signal at 400 eV can be assigned to the N—O species[29,30]. By analogy, the peak at 400.0 eV in g-C_3N_4/NGQDs/TiO_2 may be partly ascribed to the formation of the N—O bonds between g-C_3N_4 and NGQDs(or TiO_2). Such strong interaction among g-C_3N_4, NGQDs and TiO_2 could help to widen the light absorption range and enhance the photogenerated charge carriers migrate efficiently[31].

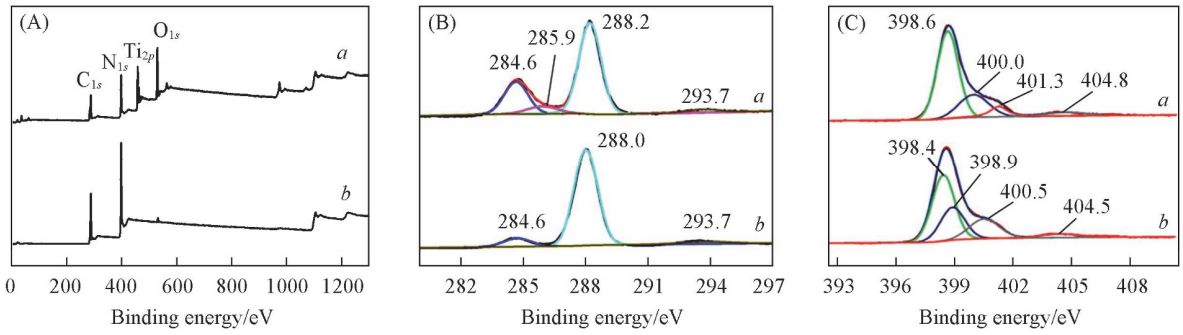

Fig.4 XPS spectra of survey(A), C_{1s}(B), and N_{1s}(C) in g-C_3N_4/NGQDs/TiO_2(*a*) and g-C_3N_4(*b*) samples

3.2 Optical and Electrochemical Properties

Fig.5 shows the UV-Vis absorption spectra of different samples. As shown in Fig.5(A), pure g-C_3N_4 exhibits an obvious absorption edge at approximately 460 nm, which is ascribed to the intrinsic band gap of g-C_3N_4[32]. Besides, the P25 exhibits outstanding UV absorption with an absorption edge at around 410 nm. There was an obvious blue shift in the absorption edge of g-C_3N_4/TiO_2 powder, compared to pure g-C_3N_4. The result is similar to what has been reported in g-C_3N_4/TiO_2 system[9,11,25]. However, after the NGQDs being introduced, the absorption band edge of g-C_3N_4/NGQDs/TiO_2 extended to around 554 nm. A red shift was generated compared with pure g-C_3N_4, In addition, a stronger tail absorption in the range of 400—800 nm was also observed due to the new band state caused by the distortions or defects in g-C_3N_4/NGQDs/TiO_2[33], which would contribute to the absorption of visible light and be favorable for the photocatalysis. The corresponding band gaps of samples can be derived according to the Kubella-Munk function. As shown in Fig.5(B), the band gaps are 3.02, 2.68, 2.74 and 2.24 eV for pure TiO_2(P25), g-C_3N_4, g-C_3N_4/TiO_2 and g-C_3N_4/NGQDs/TiO_2 samples, respectively. The as-synthesized g-C_3N_4/NGQDs/TiO_2 composite has the lowest band gap, which indicated that the intermediate band was created and more visible light would be harvested[20,34].

Fig.6(A) shows the PL spectra of different samples under the excitation wavelength of 370 nm. The pure g-C_3N_4 produced a strong characteristic emission peak located at 470 nm, which was caused by the direct recombination of electrons and holes. The PL intensity of g-C_3N_4/TiO_2 was much lower than that of g-C_3N_4, indicating that the recombination of photo-induced carriers was efficiently prohibited due to the efficient electron transfer from g-C_3N_4 to TiO_2[12]. After the introduction of NGQDs into g-C_3N_4/TiO_2, g-C_3N_4/NGQDs/TiO_2 ternary heterojunction exhibited the lowest PL emission, suggesting that it had the lowest recombination rate of photogenerated electrons-holes pairs. This could be explained by the good electron transfer function of NGQDs. In addition, the PL emission of g-C_3N_4/NGQDs/TiO_2 showed serious trailing from 480 nm tp 700 nm, indicating the strong interaction among NGQDs, g-C_3N_4 and TiO_2.

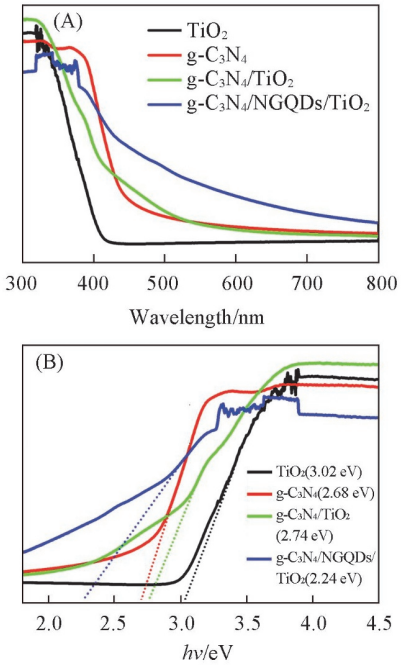

Fig.5 UV-Vis absorption spectra(A) and band gaps(B) of pure g-C_3N_4, TiO_2(P25), g-C_3N_4/TiO_2 and g-C_3N_4/NGQDs/TiO_2 samples

EIS was also measured to study the separation and mobility of photogenerated charges. In the EIS Nyquist plot, the smaller semicircle arc corresponds to the easier charge transfer[22]. EIS plots of g-C_3N_4/NGQDs/TiO_2 sample showed a smaller arc size than those of pure g-C_3N_4, TiO_2(P25) and g-C_3N_4/TiO_2 samples[Fig.6(B)], indicating that it had a faster interfacial charge transfer performance. The results from PL spectra and EIS plots confirmed that NGQDs as a charge transfer mediator between g-C_3N_4 and TiO_2 enhanced the electron transfer and reduced the charge recombination[35].

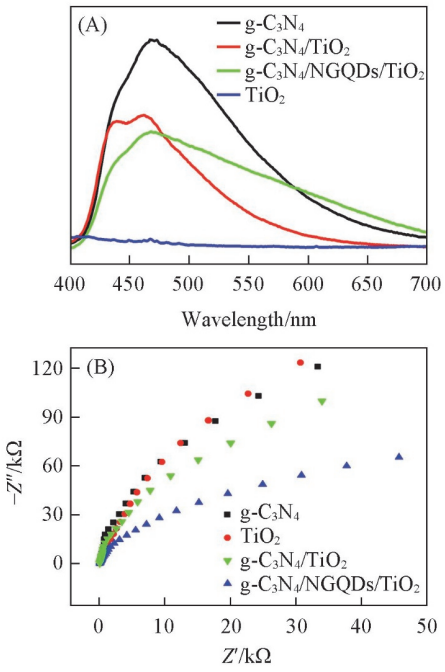

Fig.6 PL spectra(A) and EIS Nyquist plots(B) of pure g-C_3N_4, TiO_2(P25), g-C_3N_4/TiO_2 and g-C_3N_4/NGQDs/TiO_2 samples

3.3 Photocatalytic Performance

The photocatalytic performance of the as-prepared samples was evaluated by the degradation of CIP in water under visible light irradiation. Fig.7(A) shows the influence of different P25 proportions in the g-C_3N_4/NGQDs/TiO_2 composites on the photocatalytic activities for CIP degradation with a fixed mass ratio of NGQDs:urea=6:10000. The photocatalytic activities of the composites increased as the relative mass ratio of P25 over urea increased from 0 to 5:100(Table 1). However, a subsequent increase of the relative mass ratio to 10:100 led to a decrease in CIP degradation efficiency. This could be explained

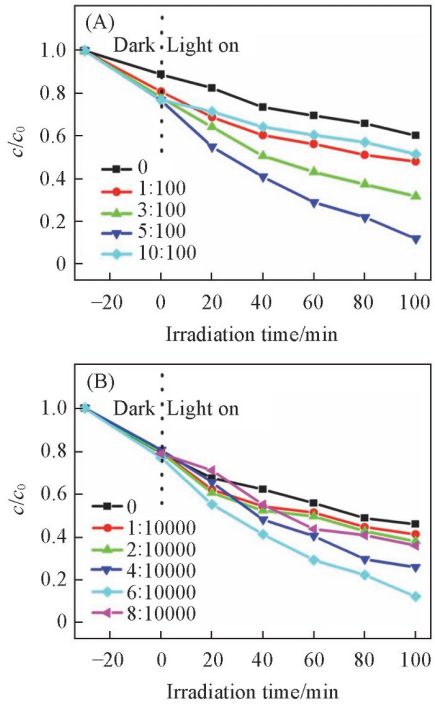

Fig.7 Visible-light driven degradation of CIP by g-C_3N_4/NGQDs/TiO_2 composites prepared with different mass ratios of P25 over urea, among which the mass ratio of NGQDs over urea was fixed at 6:10000(A) and with different mass ratios of NGQDs over urea, among which the mass ratio of P25 over urea was fixed at 5:100 in the precursors(B)

by the reason that redundant P25 might cover the active sites of g-C_3N_4 and hinder the visible-light penetration to g-C_3N_4/NGQDs/TiO_2 composite[9]. Therefore, g-C_3N_4/NGQDs/TiO_2 composite with a mass ratio of 5:100 for P25 over urea exhibited highly efficient photocatalytic activity.

Fig.7(B) shows the effect of different mass ratios of NGQDs over urea in the g-C_3N_4/NGQDs/TiO_2 composite on the photocatalytic performance with a fixed mass ratio of P25:urea=5:100. It was found that when NGQDs were introduced into the g-C_3N_4 and TiO_2 system, g-C_3N_4/NGQDs/TiO_2 ternary heterojunction exhibited more remarkably enhanced photocatalytic activity compared with g-C_3N_4/TiO_2[denoted as the mass ratio of NGQDs:urea=0 in Fig.7(B)]. Obviously, when the mass ratio of NGQDs over urea reached 6:10000, g-C_3N_4/NGQDs/TiO_2 composite displayed the highest photocatalytic activity(Table 1). Nevertheless, the CIP degradation rate decreased when the NGQDs content further increased because too many NGQDs might shield the composite from absorbing visible light[36,37]. In general, the optimal mass ratios of P25:urea and NGQDs:urea were 5:100 and 6:10000, respectively, in the precursors for the preparation of g-C_3N_4/NGQDs/TiO_2 heterojunction, and the corresponding mass fractions of TiO_2, g-C_3N_4 and NGQDs were calculated to be about 68%, 31.2% and 0.8%, respectively, based on the above TGA result.

The photocatalytic activity of optimal g-C_3N_4/NGQDs/TiO_2 heterojunction was compared with pure g-C_3N_4, TiO_2(P25) and g-C_3N_4/TiO_2. As observed in Fig.8(A), the photolysis of CIP without any photocatalyst can be ignored according to the blank experiment. The pure g-C_3N_4 and TiO_2(P25) possessed relatively low photocatalytic performance, and only 27.7% and

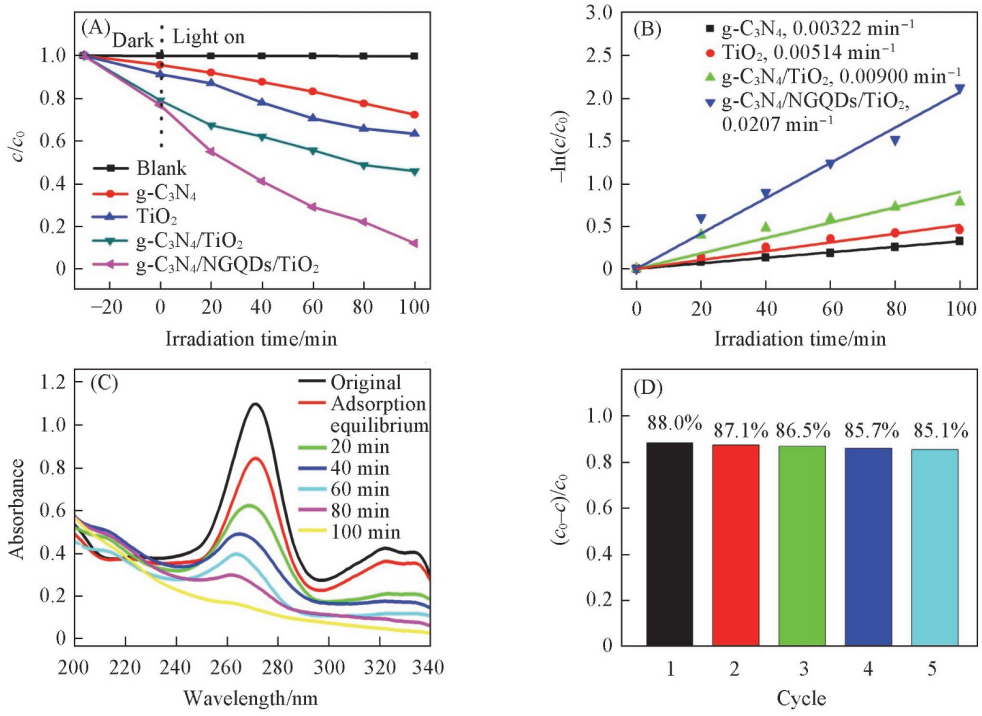

Fig.8 Photocatalytic degradation of CIP with the as-prepared photocatalysts under visible light(A), the pseudo-first-order rate constants of CIP photodegradation under visible light(B), the variation of CIP main absorption peak with irradiation time over g-C_3N_4/NGQDs/TiO_2 sample(C) and the recycling photocatalytic tests of g-C_3N_4/NGQDs/TiO_2 sample(D)

36.7% of CIP were degraded upon 100-min visible light irradiation, respectively. The g-C_3N_4/TiO_2 binary heterojunction remarkably promoted the photocatalytic efficiency and 54.2% of CIP could be degraded at the same time by g-C_3N_4/TiO_2 composite. Nevertheless, when NGQDs were introduced into g-C_3N_4/TiO_2, the g-C_3N_4/NGQDs/TiO_2 ternary heterojunction exhibited the highest photocatalytic activity among the tested samples, and 88.0% of CIP were degraded in 100 min under visible light irradiation.

Fig.8(B) demonstrates the reaction kinetic of photocatalytic degradation CIP by different photocatalysts. It can be observed that the changes of the CIP concentration *vs.* the irradiation time for these samples conformed to the following pseudo-first-order kinetics: $-\ln(c/c_0)=kt$, where c_0 and c are the concentrations of CIP at times 0 and t, respectively, and k is the apparent rate constant(min^{-1}). As shown in Fig.8(B), the k value of g-C_3N_4/NGQDs/TiO_2 is 0.0207 min^{-1}, which is 6.43, 4.03 and 2.30 times higher than those of g-C_3N_4(0.00322 min^{-1}), TiO_2(0.00514 min^{-1}) and g-C_3N_4/TiO_2(0.00900 min^{-1}), respectively. Fig.8(C) shows the variation of UV-Vis absorption spectra of CIP degradation over optimal g-C_3N_4/NGQDs/TiO_2 heterojunction under visible light illumination, in which the intensity of characteristic absorption peak of CIP at 272 nm decreased with increasing the irradiation time. Besides, the photocatalytic stability of g-C_3N_4/NGQDs/TiO_2 was also investigated by repetitive use experiments. As shown in Fig.8(D), the degradation rate of g-C_3N_4/NGQDs/TiO_2 sample is still higher than 85% after five cycles, which confirms the satisfying stability and recyclability of the g-C_3N_4/NGQDs/TiO_2 photocatalyst.

Photocatalytic experiments indicated a synergetic effect among g-C_3N_4, NGQDs and TiO_2. This triple g-C_3N_4/NGQDs/TiO_2 heterojunction prepared by one-step heat treatment facilitated intimate interfacial interactions among three functional unit phases. The NGQDs were firstly covalently linked with g-C_3N_4 to form g-C_3N_4/NGQDs by the deamination reaction of g-C_3N_4 precursor urea and NGQDs according to our previous report[20], and then to further form g-C_3N_4/NGQDs/TiO_2 heterojunction by calcining the g-C_3N_4/NGQDs and TiO_2. NGQDs could act as a bridge to connect g-C_3N_4 and TiO_2[38]. The enhanced photocatalytic performance of g-C_3N_4/NGQDs/TiO_2 could be explained by the reason that the introduction of NGQDs enhanced visible light absorption ability and facilitated faster interfacial charge transfer and more efficient separation of photogenerated electrons and holes[36,39,40], which had been evidenced by the aforementioned UV-Vis absorption spectra, PL and EIS study.

The species trapping experiments were carried out to speculate the photocatalytic mechanism(Fig.9). The photocatalytic efficiency was not obviously changed with the addition of IPA to trap $^{\bullet}OH$[37]. On the country, the photocatalytic activities were substantially inhibited by different degree after adding TEOA and BQ to the reaction solution to trap holes(h^+) and $^{\bullet}O_2^-$[18,41], respectively, which suggested that $^{\bullet}O_2^-$ and h^+ were the major reactive species for CIP degradation under visible light illumination.

On the basis of the above results and discussion, a reasonable photocatalytic mechanism for the g-C_3N_4/NGQDs/TiO_2 composite is tentatively proposed as illustrated in Scheme 1. The excellent photocatalytic activity of g-C_3N_4/NGQDs/TiO_2 may be attributed to narrow band gap and high charge carrier mobility compared to pure g-C_3N_4, TiO_2(P25) and g-C_3N_4/TiO_2. The electronic coupling between NGQDs and g-C_3N_4 by the deamination reaction could generate new bands, extending the visible light response range. This behavior was proved and discussed in our previous work[20] and the aforementioned UV-Vis absorption spectra. Under visible light irradiation, the photogenerated electrons of NGQDs/g-C_3N_4 can not only transfer to the conduction band(CB) of g-C_3N_4, but also be directly injected into new energy bands. The excited electrons in the CB or new energy bands of g-C_3N_4 could simply migrate to NGQDs and then transfer to CB of TiO_2, resulting in further improvement of the charge separation efficiency, which was driven by the excellent electron acceptor and donor properties of NGQDs. The electrons in the CB of TiO_2 could react with the O_2 to yield $^{\bullet}O_2^-$ reactive species, which could degradate CIP. Additionally, the h^+ in the valence band (VB) of g-C_3N_4 would react with CIP straightly and take part in the photodegradation of CIP.

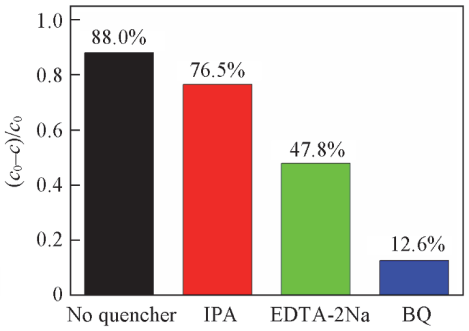

Fig.9 Species trapping experiments for CIP degradation over g-C_3N_4/NGQDs/TiO_2 under visible light irradiation

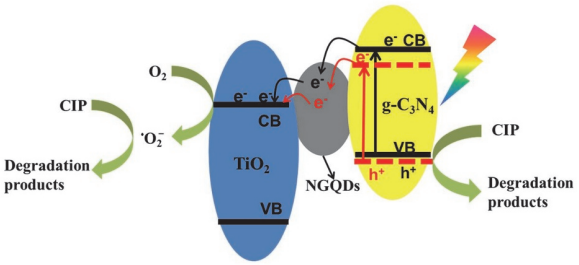

Scheme 1 Plausible diagram for separation of electron-hole pairs in the g-C_3N_4/NGQDs/TiO_2 composite

4 Conclusions

In conclusion, a series of ternary g-C_3N_4/NGQDs/TiO_2 photocatalysts was successfully fabricated by facile one-step calcining treatment, which was applied in photodegradations of CIP under visible light. At the optimal content, the g-C_3N_4/NGQDs/TiO_2 composite exhibited the highest photocatalytic activity toward CIP degradation, the apparent rate constant of which was almost 6.43, 4.03 and 2.30 times higher than those

of g-C_3N_4, TiO_2 and g-C_3N_4/TiO_2, respectively. The enhancement of the photocatalytic performance should be attributed to the synergistic effect of promoting the separation of photogenerated carriers and improving light harvesting with the construction of g-C_3N_4/NGQDs/TiO_2 ternary heterojunction. This ternary composite material would be a promising photocatalyst for the practical applications in the antibiotics and organic pollutant degradation.

References

[1] Välitalo P., Kruglova A., Mikola A., Vahala R., *Int. J. Hyg. Environ. Health*, **2017**, *220*, 558

[2] Lin J.-S., Pan H.-Y., Liu S.-M., Lai H.-T., *J. Environ. Sci. Heal. B*, **2010**, *45*, 456

[3] Li D., Shi W., *Chinese J. Catal*., **2016**, *37*, 792

[4] Liao G., Gong Y., Zhang L., Gao H., Yang G.-J., Fang B., *Energ. Environ. Sci.*, **2019**, *12*, 2080

[5] Reddy K. R., Reddy C. H. V., Nadagouda M. N., Shetti N. P., Jaesool S., Aminabhavi T. M., *J. Environ. Manage.*, **2019**, *238*, 25

[6] Zada A., Qu Y., Ali S., Sun N., Lu H., Yan R., Zhang X., Jing L., *J. Hazard. Mater.*, **2018**, *342*, 715

[7] Schneider J., Matsuoka M., Takeuchi M., Zhang J., Horiuchi Y., Anpo M., Bahnemann D. W., *Chem. Rev.*, **2014**, *114*, 9919

[8] Xu Y., Luo Y., Qian Q., Huang B., Chen Q., *Opt. Mater.*, **2017**, *72*, 691

[9] Chen P., Wang F., Zhang Q., Su Y., Shen L., Yao K., Chen Z.-F., Liu Y., Cai Z., Lv W., Liu G., *Chemosphere*, **2017**, *172*, 193

[10] Wang H., Li J., Ma C., Guan Q., Lu Z., Huo P., Yan Y., *Appl. Surf. Sci.*, **2015**, *329*, 17

[11] Yang Z., Yan J., Lian J., Xu H., She X., Li H., *ChemistrySelect*, **2016**, *1*, 5679

[12] Sheng Y., Wei Z., Miao H., Yao W., Li H., Zhu Y., *Chem. Eng. J.*, **2019**, *370*, 287

[13] Acharya R., Parida K., *J. Environ. Chem. Eng.*, **2020**, *8*, 103896

[14] Zhang Z., Zhang J., Chen N., Qu L., *Energ. Environ. Sci.*, **2012**, *5*, 8869

[15] Wang Z., Zeng H., Sun L., *J. Mater. Chem. C*, **2015**, *3*, 1157

[16] Liu J., Xu H., Xu Y., Song Y., Lian J., Zhao Y., Wang L., Huang L., Ji H., Li H., *Appl. Catal. B: Environ.*, **2017**, *207*, 429

[17] Xu T., Wang D., Dong L., Shen H., Lu W., Chen W., *Appl. Catal. B: Environ.*, **2019**, *244*, 96

[18] Yan M., Zhu F., Gu W., Sun L., Shi W., Hua Y., *RSC Adv.*, **2016**, *6*, 61162

[19] Tang L., Ji R., Li X., Teng K. S., Lau S. P., *J. Mater. Chem. C*, **2013**, *1*, 4908

[20] Mou Z., Lu C., Yu K., Wu H., Zhang H., Sun J., Zhu M., Goh M. C., *Energy Technol.*, **2019**, *7*, 1800589

[21] Qu D., Zheng M., Du P., Zhou Y., Zhang L., Li D., Tan H., Zhao Z., Xie Z., Sun Z., *Nanoscale*, **2013**, *5*, 12272

[22] Guo F., Chen J., Zhao J., Chen Z., Xia D., Zhan Z., Wang Q., *Chem. Eng. J.*, **2020**, *386*, 124014

[23] Zhang L., Xi Z., Xing M., Zhang J., *Int. J. Hydrogen Energ.*, **2013**, *38*, 9169

[24] Yu J., Wang S., Low J., Xiao W., *Phys. Chem. Chem. Phys.*, **2013**, *15*, 16883

[25] Pan J., You M., Chi C., Dong Z., Wang B., Zhu M., Zhao W., Song C., Zheng Y., Li C., *Int. J. Hydrogen Energ.*, **2018**, *43*, 6586

[26] He J., Sun H., Indrawirawan S., Duan X., Tade M. O., Wang S., *J. Colloid Interf. Sci.*, **2015**, *456*, 15

[27] Zhang M., Lai C., Li B., Huang D., Zeng G., Xu P., Qin L., Liu S., Liu X., Yi H., Li M., Chu C., Chen Z., *J. Catal.*, **2019**, *369*, 469

[28] Ming L., Yue H., Xu L., Chen F., *J. Mater. Chem. A*, **2014**, *2*, 19145

[29] Qiu X., Zhao Y., Burda C., *Adv. Mater.*, **2007**, *19*, 3995

[30] Zhong R., Zhang Z., Yi H., Zeng L., Tang C., Huang L., Gu M., *Appl. Catal. B: Environ.*, **2018**, *237*, 1130

[31] Zhong R., Zhang Z., Luo S., Zhang Z. C., Huang L., Gu M., *Catal. Sci. Technol.*, **2019**, *9*, 75

[32] Fu J., Yu J., Jiang C., Cheng B., *Adv. Energy Mater.*, **2018**, *8*, 1701503

[33] Zhao W., Hao N., Zhang G., Ma A., Chen W., Zhou H., Yang D., Xu B. B., Kong J., *Chem. Res. Chinese Universities*, **2020**, *36*(6), 1271

[34] Li C., Sun Z., Zhang W., Yu C., Zheng S., *Appl. Catal. B: Environ.*, **2018**, *220*, 272

[35] Ding Y., Gao Y., Li Z., *Appl. Surf. Sci.*, **2018**, *462*, 255

[36] Che H., Liu C., Hu W., Hu H., Li J., Dou J., Shi W., Li C., Dong H., *Catal. Sci. Technol.*, **2018**, *8*, 622

[37] Yan M., Hua Y., Zhu F., Gu W., Jiang J., Shen H., Shi W., *Appl. Catal. B: Environ.*, **2017**, *202*, 518

[38] Wang B., Ding Y., Deng Z., Li Z., *Chinese J. Catal.,* **2019,** *40*, 335

[39] Zhu M., Liu Q., Chen W., Yin Y., Ge L., Li H., Wang K., *ACS Appl. Mater. Inter.*, **2017**, *9*, 38832

[40] Wang B., Deng Z., Fu X., Li Z., *J. Mater. Chem. A*, **2018**, *6*, 19735

[41] Asadzadeh-Khaneghah S., Habibi-Yangjeh A., Yubuta K., *J. Am. Ceram. Soc.*, **2019**, *102*, 1435